Discover Geoscience

Research

Geo-electrical prognosis of aquifer protectivity, corrosivity, and vulnerability via index-based models within a major coastal milieu

Ndifreke I. Udosen[1] · Aniekan M. Ekanem[1] · Nyakno J. George[1]

Received: 15 February 2024 / Accepted: 7 June 2024
Published online: 11 June 2024

Abstract
This work was carried out to investigate the protective capacity, vulnerability, and corrosivity within a major coastal milieu in Southern Nigeria with the use of index-based geo-electrical modeling methods. Vertical electrical soundings were undertaken at twenty locations with the aid of Schlumberger array having a maximum electrode spacing of 400 m. The results indicated that the lithology comprised four subsurface layers having variable values of resistivity and thickness. The Dar-Zarrouk parameter, the Aquifer Vulnerability Index (AVI), and the GOD (Groundwater occurrence G, Overlying lithology O and Depth to aquifer D) models were employed to appraise measures of aquifer protectivity and vulnerability to contamination. The longitudinal conductance values ranged from 0.0071–1.95 mhos with a mean of 0.32 mhos, indicating moderate protectivity. AVI values ranged from 1.73–4.10 with a mean of 3.03, indicating moderate aquifer vulnerability. The GOD indices ranged from 0.35–0.63 with a mean of 0.49, indicating moderate aquifer vulnerability. Corrosivity was also computed based on topsoil resistivity values which ranged from 12.7 to 664.2 Ωm with a mean of 168.17 Ωm, indicating moderate corrosivity, and demonstrating the unsuitability of corrosive locations for laying underground pipes. All the index-based models gave similar interpretations, indicating moderate aquifer protectivity and susceptibility. These results were corroborated by 2D electrical resistivity tomography surveys conducted at four stations. This work has therefore delineated important aquifer geo-hydraulic properties with index-based geo-electrical modeling techniques. The results obtained are critical for effective aquifer management, conservation, and sustainability.

Keywords Aquifer vulnerability index (AVI) model · GOD vulnerability model · Longitudinal conductance · Corrosivity · Electrical resistivity · Vertical electrical sounding

1 Introduction

Water is related to various parts of the hydrologic cycle. It arrives the earth surface in the form of precipitation and snowmelts, and during runoff, it percolates the subsurface, employing gravitational forces to infiltrate permeable geo-layers [1]. Groundwater accumulates within the phreatic or saturated zone underlying the vadose zone, which is the zone of partial water saturation [2, 3]. The water table (top of the aquiferous zone) could either be high (implying shallowness to the near surface) or low (implying greater depth). High water tables are common during periods of heavy rainfall, snow or ice melts, while low water tables are typical during arid seasons [4]. Subterranean water

✉ Ndifreke I. Udosen, ndifreke.udosen@yahoo.com; ndifrekeudosen@aksu.edu.ng | [1]Department of Physics, (Geophysics Research Group), Akwa Ibom State University, Mkpat Enin, Nigeria.

flow via porous and permeable rocks trends from zones of high elevation and pressure to zones of low elevation and pressure, implying movement from regions of high hydraulic head to regions of low hydraulic head. The larger the hydraulic head difference, the faster the groundwater flow rate or discharge [5] as expressed by Darcy's law

$$Q = K \cdot A \frac{\Delta h}{\Delta l} \quad (1)$$

where Q is the groundwater discharge, K is the hydraulic conductivity, A is the cross-sectional area, $\frac{\Delta h}{\Delta l}$ is the hydraulic gradient (hydraulic head difference).

Groundwater is considered a viable source of potable water compared to surface water resources. This is because as groundwater passes through soil and rock formations, it undergoes filtering, leading to the elimination of contaminants like rock sediments and micro-organisms, although some dissolved solids and toxicants are difficult to purify naturally despite huge depths of subsurface travel [4, 5]. The filtering capacity of soil and rock is influenced by rock minerology and composition. For example, sewage is filtered at approximately 30-45 m during percolation when it travels through sandy loam and organic humus [5]. The filtering process is undertaken via decomposition and ion absorption by humus and argillitic minerals. On the other hand, highly fractured granitic/limestone rocks (which are highly permeable) are incapable of purifying sewage even at very great depths of travel owing to the rapidity of fluid/material flow through such rock materials [5]. Sources of groundwater pollution include pesticides, fertilizers, organic manure, and herbicides employed during agricultural activities. Other sources are sewage, oil spills, saltwater intrusion, industrial acid mine drainage, and leachate from landfills [2, 4–8] Groundwater pollution is especially insidious since its damaging impacts are not easily evident. Percolation of contaminants takes place within rocks, not land, hence it may take a long time for contamination to be detected. The slow rate of groundwater's travel through subsurface rocks generates time lapses between the period when a contaminant product starts its journey within the vadose zone, to when it finally ends in the aquifer system. This makes pollutant detection more difficult [2, 4]. How susceptible groundwater is to contamination is influenced by regional geology, nature of contaminant material, and length of stay of groundwater within the aquifer before its extraction. The shorter the length of groundwater's stay prior to extraction (e.g., in shallow aquifers), the less the opportunity for moderation and filtration of toxic contaminants, leading to greater concentrations of toxicity [2, 4, 5]. It is therefore important that groundwater pollution be prevented in the first place, as its cleanup procedures are more difficult and expensive compared to cleanup of surface water sources [2, 4]. Preventative and responsive methods are required to safeguard local water systems. However, from a financial viewpoint, preventative methods are superior to reactive methods, as reactiveness implies higher cost and more challenging cleanup, and in some cases, it may be impractical [2, 8].

One of such preventative approaches involves the generation of groundwater models and maps to indicate regions of vulnerability. Groundwater vulnerability models delineate indices within an aquifer system that determines to what extent groundwater quality will be degraded by an introduced pollutant [9]. Several factors affect groundwater vulnerability. These include the type of groundwater confinement, the lithology of the overburden strata, the depth to the water table, the attenuation capacity of the pollutants as it moves through the vadose zone, the thickness of the overburden, and the hydraulic conductivity within the water bearing formations [10–13]. With the burgeoning population in the study area located in Southern Nigeria, coupled with increasing rates of urbanization and industrialization, groundwater resources (which happens to be the sole potable water source in the region) is highly predisposed to contamination as a result of anthropogenic activities. Not only must new groundwater sources be found and exploited to supply the current water needs of a growing population, safeguards also have to be applied to protect dwindling water supplies from contamination. Availability of potable surface or groundwater resources is a basic requirement, impacting extent of economic development within nations, and facilitating the achievement of UN Sustainable Development Goals [14–16].

To ensure a continuous supply of safe potable water in the study area, geophysical methods [17–24] were undertaken to investigate the extent of aquifer susceptibility to contamination. These geophysical techniques have the ability to detect variation in properties like electromagnetic and resistivity distribution within the earth's surface [25–29]. The reason these methods have been a preferred choice in groundwater investigation and other environmental research projects is because of their portability, non-invasiveness, ease/rapidity of data acquisition, and reduced ambiguity with regards to measurement interpretation [30–35]. Geo-electrical techniques, for example, inject direct current into the earth via current electrodes and measure the resulting potential difference via potential electrodes to generate measures of subsurface apparent resistivity which are later inverted to generate true earth resistivity values. The variation in soil resistivity is then employed to generate tomographic images delineating subsurface electro-stratigraphy [36–39]. The geo-resistivity values generated are influenced by soil permeability, porosity, pore fluid ionic content, and mineralization of clay particles within the subsurface [40, 41]. Contrasts in geo-electrical properties within a region can delineate the geoelectric layers, identify locations of aquiferous sequences, evaluate susceptibility of the aquifer to contamination, and generate vulnerability indices for the aquifer.

Characterization of aquifer vulnerability can be undertaken using statistical models, process-based computer models, or index-based models [42–47]. Statistical models measure the chance of a given pollutant surpassing a given concentration. Process-based computer models are used to estimate the travel times of percolating pollutants, their concentrations, and the length of time the pollutant stays within a given layer. Such methodologies are expensive and require huge datasets for the simulations to be undertaken. Index-based models, on the other hand, employ a range of parameters associated with a certain degree of vulnerability. These parameters are dissected into ranks or classes that are used to determine are used to determine the extent of contamination. This work employed index-based models: the aquifer vulnerability index (AVI) model and the groundwater confinement (G), overlaying strata (O) and depth to groundwater (D) model (abbreviated as GOD), in its assessment of aquifer vulnerability. These modelling techniques were chosen for their effectiveness in generating accurate models of aquifer vulnerability. The Aquifer Vulnerability Index (AVI) modelling technique assessed aquifer vulnerability via estimates of overburden thickness (T) and hydraulic conductivity (K) whereas the GOD technique assessed aquifer vulnerability using measures of groundwater confinement (G), lithology of overburden (O) and depth to water table (D). In addition, a Dar-Zarrouk parameter (longitudinal conductance) was used to complement the index-based modeling techniques by generating measures of aquifer protectivity rating.

The goal of this research therefore, was to employ geo-electrical technology in the evaluation of aquifer vulnerability and protectivity using AVI models, GOD models, and Dar-Zarrouk parameters. The study also aimed at appraising the corrosivity of the overburden layers. Corrosivity is an important measure since high topsoil corrosivity would cause damage to underground pipes/utilities, resulting in percolation of toxic pipeline materials into subterranean water resources. The results obtained from geo-electrical surveying will be applied in the identification of lithological and geologic formations. The increasing population in the region, coupled with high rates of industrialization and urbanization, has exerted intense pressure on available water resources, necessitating this study. Zones of groundwater susceptibility would be mapped to aid in monitoring pollution-related problems. Though groundwater is exposed to other risks such as over-abstraction, drought, etc., the focus here was contamination. Mapping and modelling of groundwater vulnerability to contamination is critical for its management and conservation.

2 Geology of study area

The study area is located in Mkpat Enin, Akwa Ibom, Nigeria between latitudes 4.614° and 4.628° N, and longitudes 7.500° and 7.783° E (Fig. 1). The region is bounded on the north by Oruk Anam Local Government Area, on the south by Eastern Obolo Local Government Area, on the East by Onna Local Government Area, and on the west by Ikot Abasi Local Government Area. The region has an average elevation of 186 m above sea level and an equatorial climate comprising two major seasons: the rainy season (April to October) and the dry season (November to February) with a short harmattan spell between December and January [48, 49]. The mean annual rainfall in the region is approximately 3549 mm and the mean annual temperature is between 25 and 30°, though temperatures during the dry season do rise to values as high as 35 °C [48]. The region is drained by the Cross-River, Kwa-Iboe River, Imo River and their tributaries. The geology of the region comprises Tertiary-Quaternary Coastal Plain Sands, otherwise termed the Benin Formation, which is the uppermost layer of the Niger Delta sedimentary formation [50, 51]. Benin Formation is the major hydrogeological unit in Nigeria's Niger Delta Region [52] and constitutes more than 80% of the region. The Benin Formation comprises fine to coarse grained arenaceous materials (which are poorly sorted at some locations), sandstones and gravels of varying thicknesses intercalated with argillites [52]. There also exists deposits of fluvial loose sands, sandy clay, alluvium, beach sands, and lagoonal sands located primarily around the riverine areas [50, 51, 53]. The Benin Formation is underlain by the paralic Agbada Formation, which is the main hydro-carbon producing unit in the Niger Delta region [51, 54]. The Agbada Formation overlies the shaly Akata Formation [53].

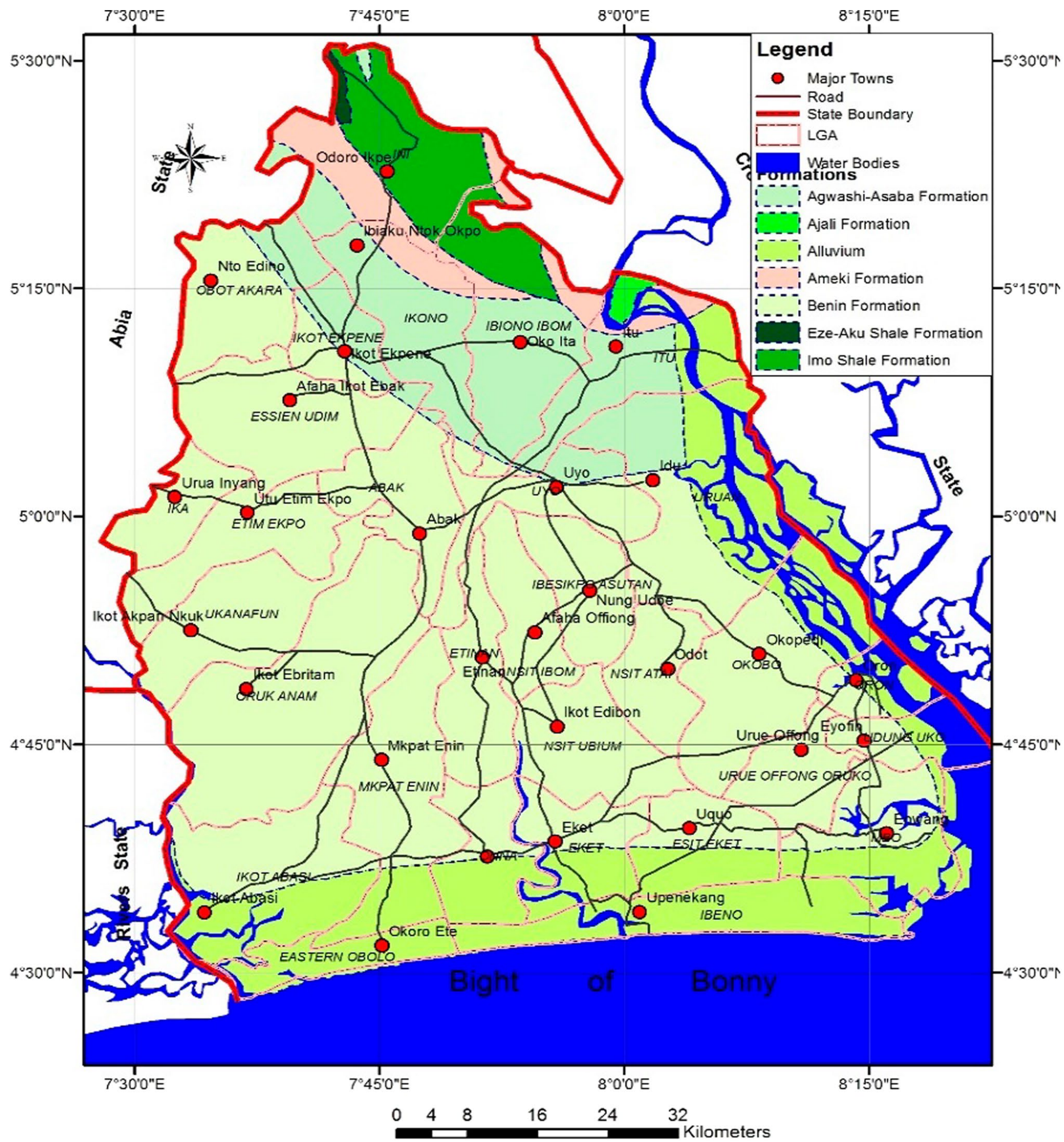

Fig. 1 Geologic map of the study area

3 Materials and methods

Geo-electrical methods were employed to acquire geo-electrostratigraphic data at twenty vertical electrical sounding (VES) stations with the ABEM SAS 1000 terrameter and its accessories. The VES stations were geo-referenced with a Global Positioning System (GPS). The Schlumberger array configuration was used. Current was injected between a pair of current electrodes A and B, and a second pair of potential electrodes M and N, was used to measure the potential difference between the current electrodes. The current electrode spacing (AB = a) was increased from 2 to 400 m, while the potential electrode spacing (MN = b) was increased from 0.5–20 m. The current electrodes were incrementally spaced out from a central point in an approximately logarithmic manner at equivalent intervals from the center, the aim being to increase the depth of current penetration. The potential electrodes were fixed while symmetrical expansions of the current electrodes were undertaken about a center. In order to generate recognizable and measurable potential readings, the potential electrode spacings were increased minutely for very large current electrode spacings. Expanding the distance between the current electrodes enabled an increment in value of the potential difference generated by the potential electrodes. In general, the MN/2 spacing had to be approximately one-fifth of the AB/2 spacing for optimal results. Schlumberger configuration was employed for its excellent depth of current penetration, its good sensitivity to vertical subsurface layers, its fast speed of data acquisition, and its mitigation of errors arising from near-surface lateral inhomogeneities [28].

Using measures of injected current and potential difference values, the terrameter employed Ohm's law

$$R_a = \frac{V}{I} \tag{2}$$

to generate measures of the apparent resistance R_a. The geometric factor of the Schlumberger array G was given by:

$$G = \pi\left(\frac{a^2}{b} - \frac{b}{4}\right) \tag{3}$$

where a is the current electrode spacing, and b is the potential electrode spacing. Values of apparent resistivity ρ_a (i.e., the mean resistivity of the geo-layer through which the injected current had travelled) were generated by multiplying apparent resistance R_a by the geometric G factor such that

$$\rho_a = \pi\left(\frac{a^2}{b} - \frac{b}{4}\right)\frac{\Delta V}{I} \tag{4}$$

Given a subsurface with homogenous and isotropic layers, the resistivity values generated from Eq. (4) would be considered as the true resistivity of the earth model. However, since the subsurface is typically heterogeneous, the true earth resistivity is dependent on the geometry of the electrode configuration employed, the spacing between the current and potential electrodes, the orientation of the electrode array with respect to subsurface heterogeneities, and the spatial variation of resistivity within the soil media. As the geo-layers do not always have horizontal stratification, what was generated from Eq. (4) was the apparent resistivity ρ_a and not the true earth resistivity. To generate true earth resistivity models would require inversion using a reconstruction algorithm [55] or inversion software. Prior to the employment of computer-based inversion software, bi-logarithmic graphs were generated with apparent resistivity values plotted as ordinate versus half the current electrode spacing (AB/2) plotted as abscissa. Values generated from those plots were used as input within the WINRESIST inversion software which generated inverse models via an iterative procedure that aimed to reduce the difference between the acquired field data and the theoretical data [56–58]. The iterations were undertaken for each sounding station until a root mean square error of < 5% was generated. The true earth model curves indicated the mean resistivity, thickness and depth of each geo-layer, and the curve signature.

2D electrical resistivity tomography surveys were also undertaken at four stations to complement information obtained from the vertical electrical sounding surveys. Wenner array was employed, with a minimum and maximum electrode spacing of 5 m and 105 m respectively. The electrodes were moved at 5 m intervals. A 2D inversion software, RES2DINV, was used to reconstruct 2D resistivity tomograms that would delineate the resistivity, thickness, and depth variations within the geo-layers.

4 Results and discussion

Table 1 illustrates the results obtained from the VES inversion curves. Figure 2 shows representative VES curves delineating the subsurface resistivity distribution. Varying curve types that delineated the spatial distribution of resistivity within the lithological layers were obtained. The geological interpretation of the inverted earth models was corroborated by results obtained from borehole logs [48]. The first layer (motley topsoil) had resistivity values ranging from 12.7 to 664.2 Ωm with a mean of 168.2 m while its thickness ranged from 0.6 to 5.3 m with a mean of 2.3 m. The second layer (sandy clay) had resistivity values ranging from 2.3 to 1203.8 Ωm with a mean of 278.5 Ωm while its thickness ranged from 1.6 to 42.7 m

Table 1 Summary of results obtained from VES inversion curves generated from WINRESIST inversion program

	Co-ordinates		Bulk Resistivity (Ωm)				Thickness (m)			Depth (m)			Elevation (m)
VES NO.	Latitude (◦)	Longitude (◦)	ρ_1	ρ_2	ρ_3	ρ_4	h_1	h_2	h_3	d_1	d_2	d_3	
1	4° 37′ 9.4″	7° 4.6′ 43.56″	425.7	103.6	1908.2	1190.1	1	12.6	92.8	1	13.6	106.4	24
2	4° 37′ 6.0″	7° 4.6′ 43.6″	212.8	741.5	232	214.7	0.7	3.2	115.5	0.7	3.9	119.4	20
3	4° 37′ 15.5″	7° 4.6′ 39.97″	222	91.6	487.9	161.1	1.1	4.2	23.7	1.1	5.3	29	15
4	4° 37′ 13.7″	7° 4.6′ 42.3″	361.1	225.5	2574	1405.6	3.6	27.6	91.1	3.6	31.2	122.3	14.5
5	4° 37′ 24.2″	7° 4.6′ 32.1″	225.5	1122.1	186.4	206.7	2.5	28.3	87.1	2.5	30.8	117.9	20
6	4° 37′ 16.6″	7° 4.6′ 18.9″	329.6	32.4	260	109.2	1.6	9.6	86.4	1.6	11.1	97.6	18
7	4° 37′ 17.4″	7° 46′ 11.4″	664.2	257.9	242.4	221.6	1.3	26.7	109.6	1.3	28	137.6	22
8	4° 37′12.3″	7° 46′29.9″	157.1	1203.8	167.8	262.6	0.6	18.1	97.8	0.6	18.7	116.5	35
9	4° 37′ 5.9″	7° 46′ 35.5″	185.5	60.9	394.2	511.1	2.1	12.6	67.5	2.1	14.7	82.2	22
10	4° 37′ 15.3″	7° 46′ 39.7″	12.7	31.8	258.1	72.8	4.3	1.8	49	4.3	6.1	55.1	13
11	4° 37′ 15.8″	7° 46′ 41.4″	51.6	495.9	160.1	463.8	2.1	15.1	72.6	2.1	17.2	89.7	15
12	4° 37′ 15.5″	7° 46′ 40.9″	21	89.5	231.1	441.3	3.3	12.6	88.3	3.3	15.6	103.9	14
13	4° 37′ 15.3″	7° 46′ 39.7″	12.7	24.8	376.7	26.1	4.1	1.6	22.7	4.1	5.7	28.4	13
14	4° 37′ 14.7″	7° 46′ 37.29″	39.8	307.6	82.9	62.9	1.5	42.7	74.3	1.5	44.2	118.6	15
15	4° 37′13.8″	7° 46′35.9″	55.2	442.5	54.3	79.4	3	17.8	82.2	3	20.8	103	26
16	4° 37′ 13.3″	7° 46′ 35.2″	113.8	251.7	514.5	60.3	5.3	14.9	45.8	5.3	20.2	66	14
17	4° 37′ 17.5″	7° 46′ 27.7″	13.4	43.1	1584	384.9	3.5	2.4	118.4	3.5	5.9	124.3	17
18	4° 37′ 16.5″	7° 46′ 22.5″	219.1	14	636.1	148	1	13.4	133.5	1	14.4	147.9	17
19	4° 37′ 16.5″	7° 46′ 19.2″	19.1	2.3	314.5	993.3	1.5	4.3	23.4	1.5	5.8	29.2	24
20	4° 37′ 15.3″	7° 46′ 44.1″	21.4	28	427	127.2	1.6	16.6	99.8	1.6	18.2	118	15

Inferred lithology from resistivity surveys constrained by lithological logs indicated that layer 1 comprised motley topsoil, layer 2 comprised sandy clay, layer 3 comprised fine sand and layer 4 comprised coarse sands. The geological interpretation of the inverted earth models was corroborated by ground truth data obtained from borehole logs [48]

with a mean of 14.3 m. The third layer (fine sand), interpreted as the aquiferous layer due to its large thickness compared to the other geo-layers, had resistivity values ranging from 54.3 to 2574.0 Ωm while the thickness ranged from 22.7 to 133.5 m with a mean of 79.1 m. The fourth layer (coarse sand) had resistivity values ranging from 26.1 m to 1405.6 Ωm with a mean of 357.1 m. Figures 3, 4 and 5 illustrates the iso-parametric maps indicating the spatial distribution of the resistivity values within the first, second and third lithological layers. To corroborate earth models generated from vertical electrical soundings, 2D resistivity tomograms obtained from electrical resistivity tomography surveys conducted at four stations were generated and the results displayed in Fig. 6a–d. The uppermost layer of the tomographic images indicated low resistivity zones, a possible result of arenite-argillitic intercalations. These low resistivity argillitic sequences reduced overburden permeability, decreasing the aquifer's susceptibility to contamination.

The Dar-Zarrouk parameter (longitudinal conductance) was employed to appraise the aquifer's protective capacity via employment of first-order geo-electrical indices. The protective capacity of an aquifer defined the overburden layer's ability to impede percolation of toxicants into the aquiferous zones. Given that the region's aquifer system is unconfined, the aquifer's primary defense against pollutant percolation were the arenite-argillitic intercalations. The low permeability of the argillitic sequences would impede pollutant infiltration and consequently protect the aquifer from contamination. Longitudinal conductance S_L was given as

$$S_L = \sum_{n}^{i=1} \frac{h_i}{\rho_i} \tag{5}$$

where ρ_i is the resistivity of ith overburden layer, h_i is the thickness of ith overburden layer, and n is the number of overburden layers.

High values of longitudinal conductance implied greater aquifer protectivity. It also meant that the overburden had a large thickness and reduced resistivity (increased conductivity). Figure 7 illustrates the iso-parametric map indicating spatial distribution of overburden thickness. The water table typically trends in the direction of terrain topography, hence

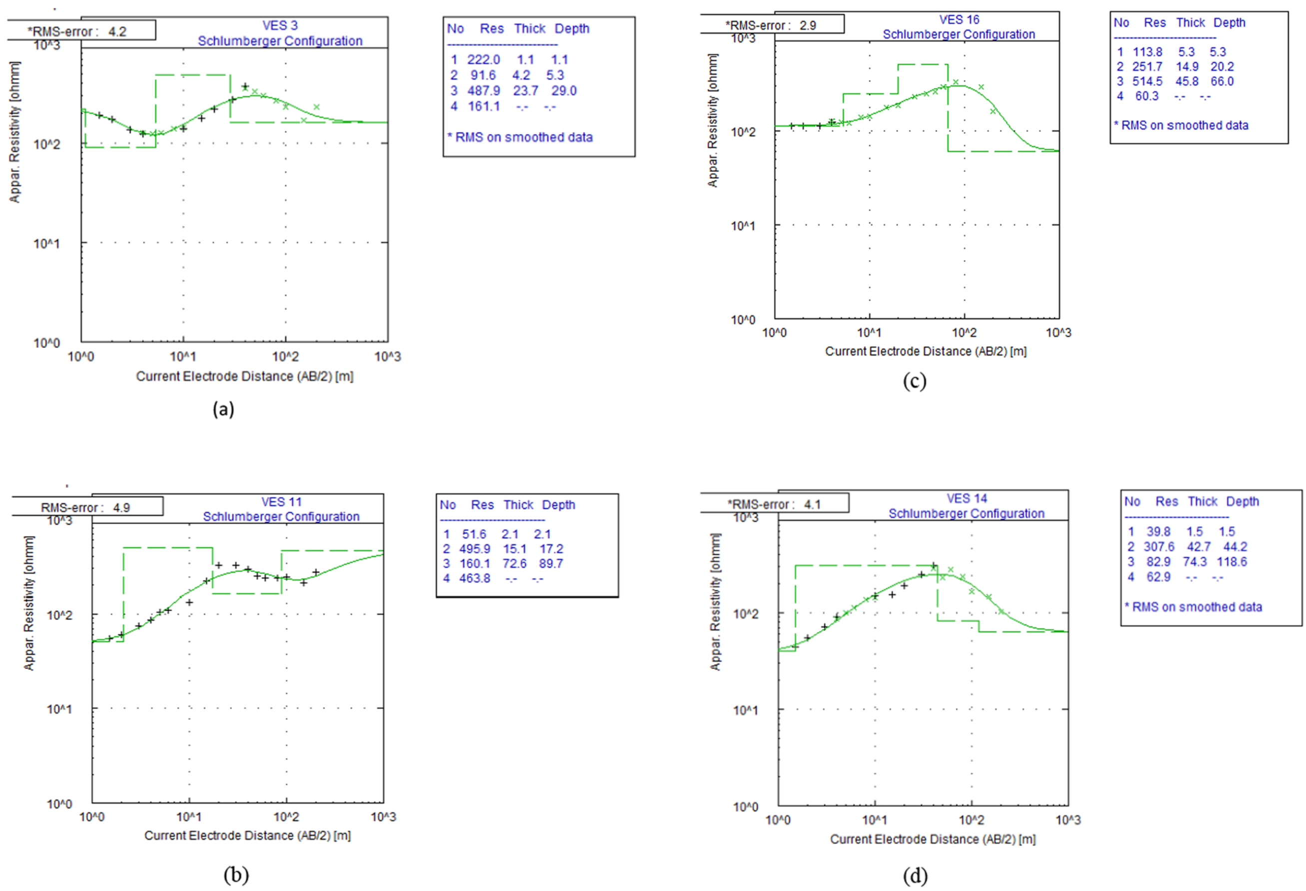

Fig. 2 a–d Representative inversion curves obtained from WINRESIST indicating measures of the first order geo-electrical indices: mean resistivity, mean thickness, and mean depth of each geo-layer

Fig. 3 Iso-parametric map indicating the spatial distribution of resistivity values within the first lithological layer (motley topsoil)

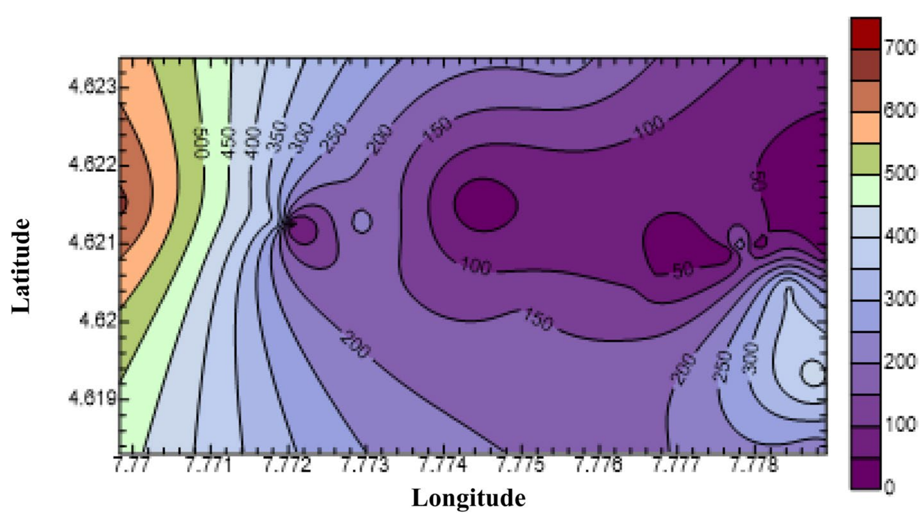

an aquifer's protective capacity would be dependent on thickness of the litho- stratigraphic layers above the water table. Formations comprising argillites or shale typically have high values of conductivity, implying greater aquifer protective rating. Pervious materials (e.g. sand and gravel) with high resistivity values have reduced ratings of aquifer protectivity. The formations in the study area comprised arenaceous materials intercalated with argillitic materials which reduced soil permeability making it difficult for contaminants to infiltrate the lithological layers [59]. The aquifer protectivity ratings based on values of longitudinal conductance values [47, 60] are shown in Table 2. Measures of longitudinal conductance

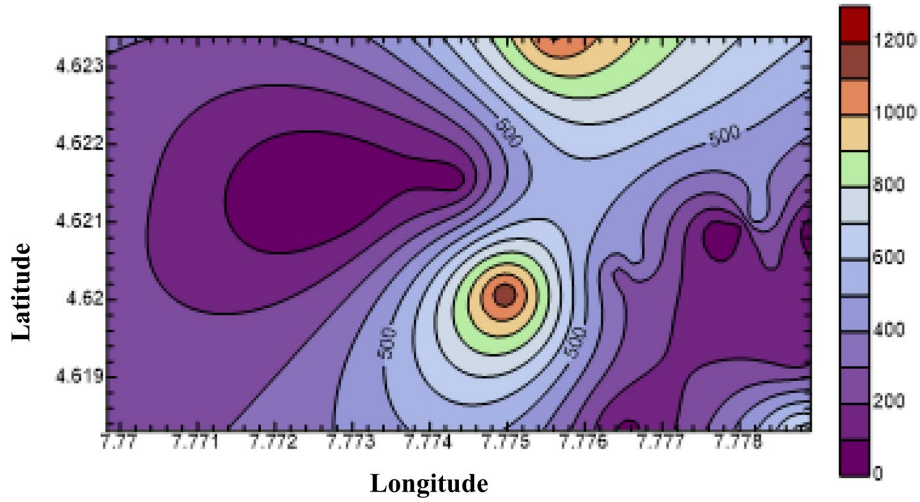

Fig. 4 Iso-parametric map indicating the spatial distribution of resistivity values within the second lithological layer (sandy clay)

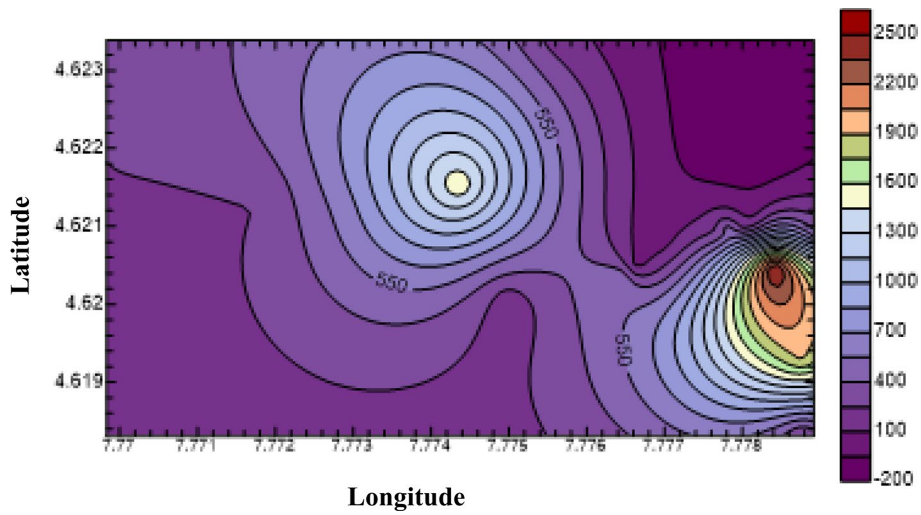

Fig. 5 Iso-parametric map indicating the spatial distribution of resistivity values within the aquiferous lithological layer (fine sand)

within the study area are given in Table 3. The table showed that longitudinal conductance values varied from 0.0076 to 1.95 mhos with a mean of 0.32 mhos, implying moderate protectivity. Locations with good protectivity indicated zones of optimal groundwater abstraction, implying that such regions were less prone to contamination. Figure 8 shows the iso-parametric map illustrating the spatial distribution of longitudinal conductance within the study area. The figure indicates that the regions within the north-east had low protectivity, resulting either from shallowness of the aquifer, thin overburden thickness, highly permeable overburden materials, or the absence of clay sequences. Such zones had a high propensity to contaminant percolation.

Most civil engineering works entail laying of pipes within the topsoil. These pipes are susceptible to corrosion when the soil media is corrosive [61]. The corrosion of underground pipes, apart from causing rusting and consequent leakage within such pipes, will leach chemicals used in pipe manufacture into the aquifer. Corrosivity is typically evaluated with measures of topsoil resistivity [61–63] (see Table 4). Corrosivity within the study are ranged from 12.7 to 664.2 Ωm with a mean of 168 0.2 Ωm, implying a gamut from practically non-corrosive to moderately corrosive (see Table 3). Figure 9 illustrated the iso-parametric map indicating the spatial distribution of corrosivity within the area. within the study area. Approximately 50% of the region was moderately corrosive, implying unsuitability of those regions for laying underground water pipes.

Index-based modelling techniques were also used to assess aquifer vulnerability to contamination. These modelling techniques were the GOD and AVI methods. These techniques did not require a plethora of parameters to give measures of groundwater vulnerability, yet they generated results as accurate as those obtained from other qualitative and quantitative methods. The GOD model [13] used the Groundwater confinement (G), overlying strata (O) and depth to

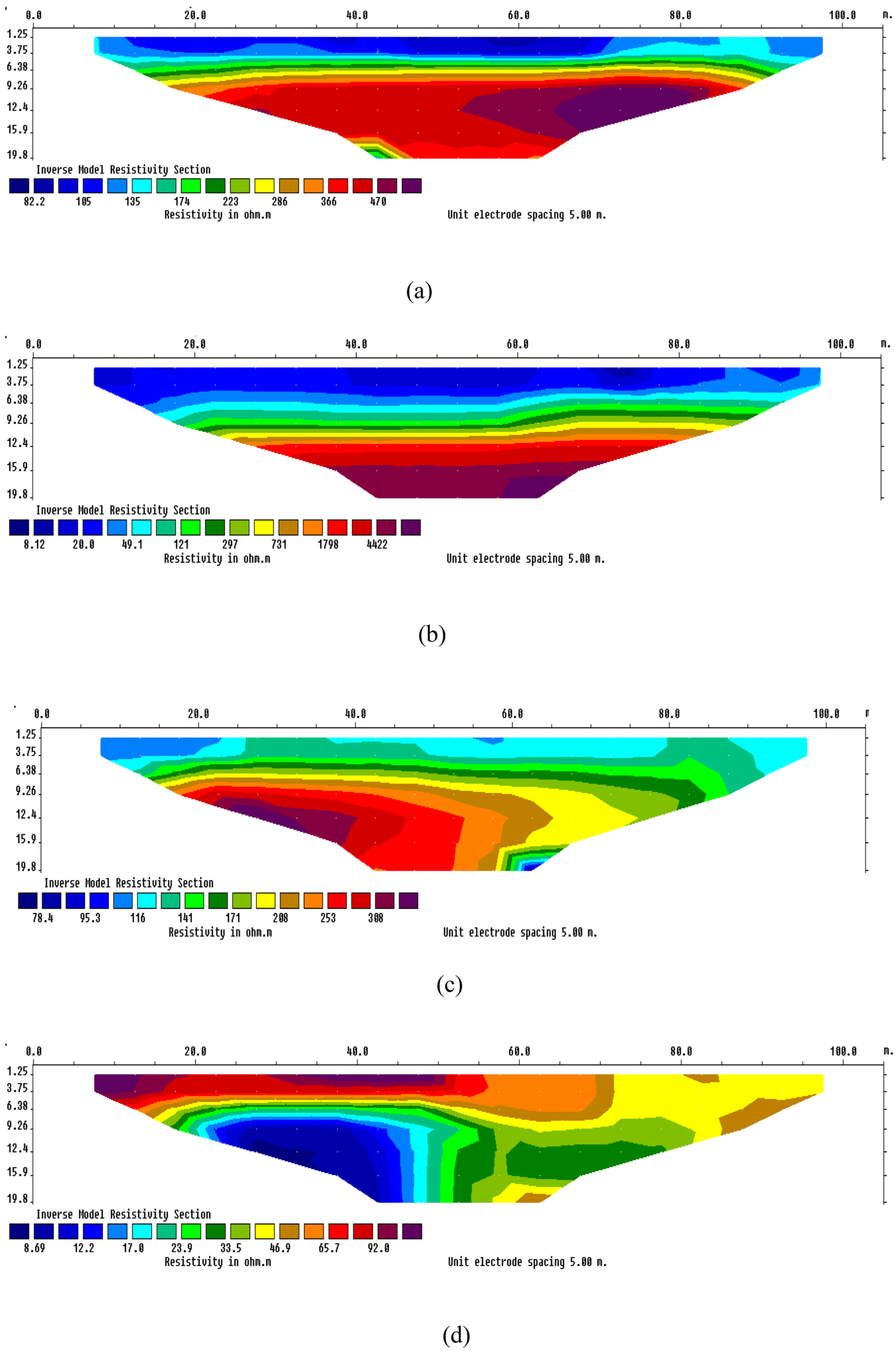

Fig. 6 **a**–**d** Spatial distribution of electrical resistivity within the survey area as generated from 2D electrical resistivity tomography surveys

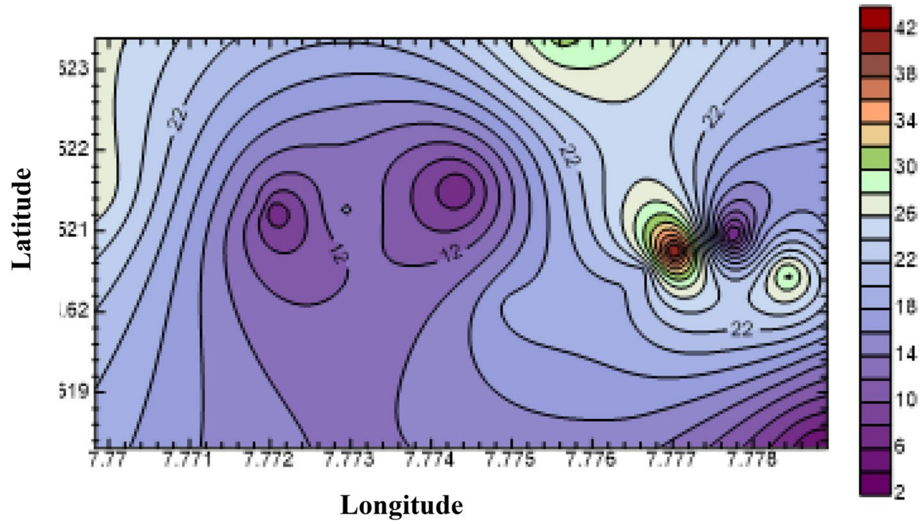

Fig. 7 Iso-parametric map indicating the spatial distribution of the overburden thickness within the study area

Table 2 Aquifer protective ratings based on values of longitudinal conductance [60]

Longitudinal conductance (mhos)	Aquifer protective capacity
> 10	Excellent
5–10	Very good
0.7–4.49	Good
0.2–0.69	Moderate
0.1–0.19	Weak
< 0.1	Poor

groundwater (D) parameters. Table 5 showed that a confined aquifer had a value of 0, while an unconfined one had a value of 1. The implication is that once an aquifer was confined, it had little or no susceptibility to contamination, and could rarely be contaminated. Confined aquifers are typically enclosed by aquitards, and have difficulty being recharged via percolation from overlying fluids. The study area, however, had an unconfined aquifer, implying that it was prone to contamination. The second parameter in the GOD model meant Overlying strata (O), i.e., the nature of overburden material overlying the aquifer. From Table 5, it was shown that the smaller the permeability of the overlying strata, the smaller the vulnerability index. The third parameter in the GOD model implied the depth to groundwater (D). Table 5 indicated that the greater the depth to groundwater, the less prone the aquifer system was to contamination, and vice versa. The overall GOD index was deduced by finding the product of the three parameters: groundwater occurrence (G), overlying strata (O) and depth to aquifer (D), such that:

$$GOD = (G) \times (O) \times (D) \tag{6}$$

The values of the GOD model indices were then used to determine the class of vulnerability based on Table 6. The GOD indices within the study area ranged from 0.35–0.63 with a mean of 0.49, implying moderate aquifer vulnerability (see Table 3). Approximately 70% of the sounding stations indicated average susceptibility ratings. The spatial distribution map of GOD values is shown in Fig. 10.

The Aquifer Vulnerability Index (AV1) modeling technique [64] was also employed to generate measures of aquifer susceptibility via computation of hydraulic resistance C such that

$$C = \sum_{i}^{n} \frac{h_i}{K_i} \quad \text{where i} = 1, 2, \ldots \text{n}. \tag{7}$$

where h_i is thickness of the ith overburden layers; K_i is the hydraulic conductivity of ith overburden layers, and n is the number of overburden layers. Equation 7 implied that high fluid flow rate (hydraulic conductivity K), would decrease the

Table 3 Measures of corrosivity, longitudinal conductance, and GOD model indices

VES NO	Latitude (◦)	Longitude (◦)	Aquifer bulk resistivity ρ_a (Ωm)	Depth to aquifer (m)	Degree of corrosivity based on resistivity of uppermost layer	Longitudinal conductance (mhos)	Aquifer protective rating	GOD Index	GOD Vulnerability rating
1	4° 37′ 9.4″	7° 4.6′ 43.56″	1908.2	13.6	Practically non-corrosive	0.123971	Weak	0.49	Average
2	4° 37′ 6.0″	7° 4.6′ 43.6″	232	3.9	Practically non-corrosive	0.007605	Poor	0.63	High
3	4° 37′ 15.5″	7° 4.6′ 39.97″	487.9	5.3	Practically non-corrosive	0.050806	Poor	0.56	High
4	4° 37′ 13.7″	7° 4.6′ 42.3″	2574	31.2	Practically non-corrosive	0.132364	Weak	0.42	Average
5	4° 37′ 24.2″	7° 4.6′ 32.1″	186.4	30.8	Practically non-corrosive	0.036307	Poor	0.42	Average
6	4° 37′ 16.6″	7° 4.6′ 18.9″	260	11.1	Practically non-corrosive	0.301151	Moderate	0.49	Average
7	4° 37′ 17.4″	7° 46′ 11.4″	242.4	28	Practically non-corrosive	0.105486	Weak	0.42	Average
8	4° 37′ 12.3″	7° 46′ 29.9″	167.8	18.7	Slightly corrosive	0.018855	Poor	0.49	Average
9	4° 37′ 5.9″	7° 46′ 35.5″	394.2	14.7	Moderately corrosive	0.218217	Moderate	0.49	Average
10	4° 37′ 15.3″	7° 46′ 39.7″	258.1	6.1	Moderately corrosive	0.395186	Moderate	0.56	High
11	4° 37′ 15.8″	7° 46′ 41.4″	160.1	17.2	Moderately corrosive	0.071147	Poor	0.49	Average
12	4° 37′ 15.5″	7° 46′ 40.9″	231.1	15.6	Moderately corrosive	0.297925	Moderate	0.49	Average
13	4° 37′ 15.3″	7° 46′ 39.7″	376.7	5.7	Moderately corrosive	0.387351	Moderate	0.56	High
14	4° 37′ 14.7″	7° 46′ 37.29″	82.9	44.2	Moderately corrosive	0.176505	Weak	0.35	Average
15	4° 37′ 13.8″	7° 46′ 35.9″	54.3	20.8	Moderately corrosive	0.094574	Poor	0.42	Average
16	4° 37′ 13.3″	7° 46′ 35.2″	514.5	20.2	Slightly corrosive	0.10577	Weak	0.42	Average
17	4° 37′ 17.5″	7° 46′ 27.7″	1584	5.9	Moderately corrosive	0.316878	Moderate	0.56	High
18	4° 37′ 16.5″	7° 46′ 22.5″	636.1	14.4	Practically non-corrosive	0.961707	Good	0.49	Average
19	4° 37′ 16.5″	7° 46′ 19.2″	314.5	5.8	Moderately corrosive	1.948099	Good	0.56	High
20	4° 37′ 15.3″	7° 46′ 44.1″	427	18.2	Moderately corrosive	0.667623	Moderate	0.49	Average

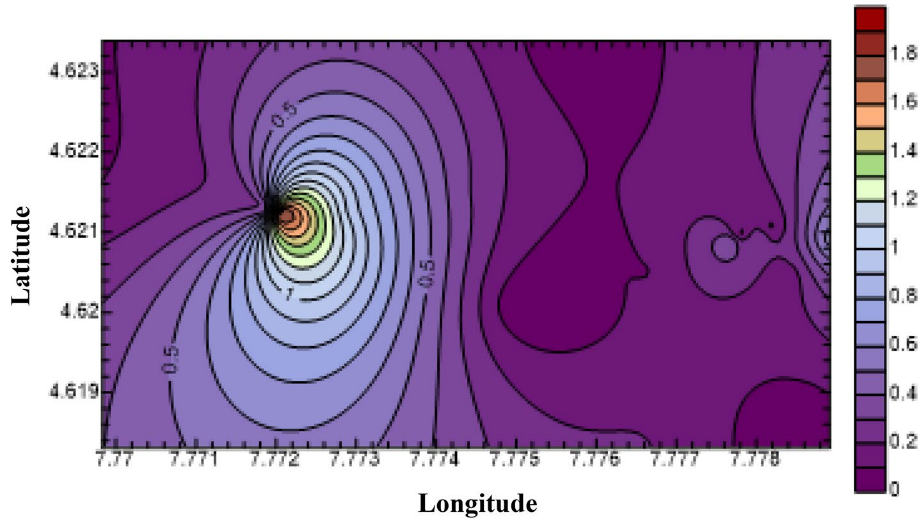

Fig. 8 Iso-parametric map indicating the spatial distribution of longitudinal conductance within the study area

Table 4 Classification of soil corrosivity based on resistivity of the topsoil [61–63]

Soil resistivity (Ωm)	Classification of soil corrosivity
< 10	Very strongly corrosive
10–60	Moderately corrosive
60–180	Slightly corrosive
> 180	Practically non-corrosive

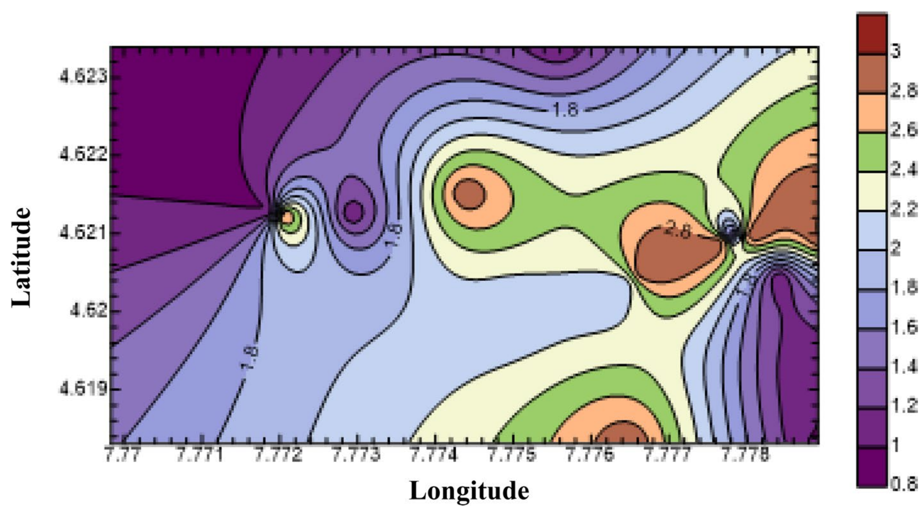

Fig. 9 Iso-parametric map indicating the spatial distribution of corrosivity within the study area. Practically non-corrosive is classified as 1, slightly corrosive is classified as 2, moderately corrosive is classified as 3, and very corrosive is classified as 4

measures of hydraulic resistance C, leading to increased aquifer vulnerability (Table 7). In addition, a small overburden thickness (h) would decrease the measures of hydraulic resistance C, increasing aquifer vulnerability. The aquifer vulnerability index (AVI) was computed by taking the logarithm of hydraulic resistance C, such that

$$AVI = \log C \tag{8}$$

The AVI values within the study area ranged from 1.73–4.10 with a mean of 3.03 (Table 8), implying moderate aquifer vulnerability. The iso-parametric map indicating the spatial distribution of the AVI values was indicated on

Table 5 Classification of GOD model indices based on the parameters: Groundwater Occurrence (G), Overlying strata (O) and Depth to groundwater (D)

Groundwater occurrence (G)	Value	Overlying strata (O)	Value	Depth to groundwater (D)	Value
Confined Aquifer	0	Sandy gravel	1	< 2	1
Un-confined Aquifer	1	Sandy gravel with sand	0.9	2–5	0.9
		Sand	0.8	5–10	0.8
		Sand with clay	0.7	10–20	0.7
		Limestone	0.6	20–40	0.6
		Silty sand	0.5	40–70	0.5
		Silty clay	0.4	70–100	0.4
		Clay	0.3	˃ 100	0.3

Table 6 Categorization of class of vulnerability based on measures of GOD indices

GOD Index	0.0–0.1	0.1–0.3	0.3–0.5	0.5–0.7	0.7–1.0
Class of vulnerability	Very low	Low	Average	High	Very high

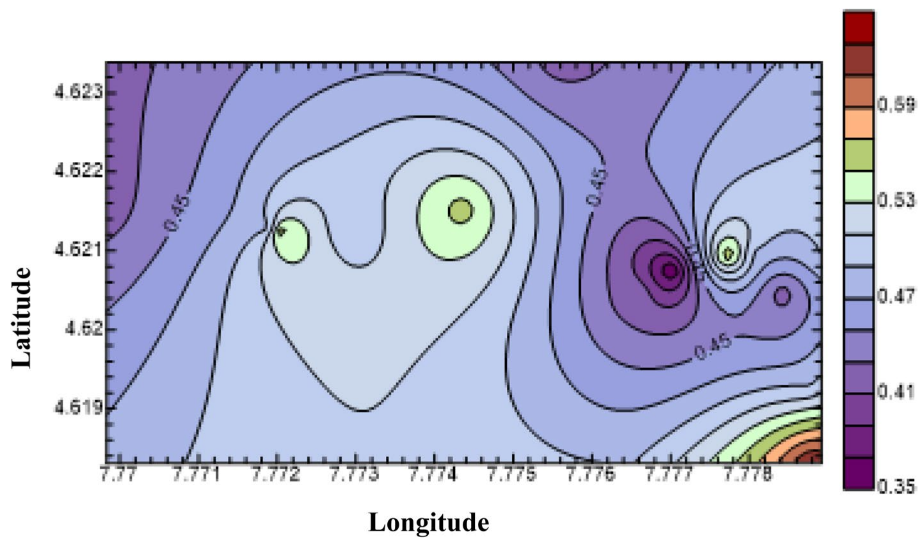

Fig. 10 Iso-parametric map indicating the spatial distribution of GOD indices within the study area

Table 7 Categorization of class of vulnerability based on measures of hydraulic resistance and AVI

Hydraulic resistance C (Ω)	AVI (Log C)	Class of vulnerability
0–100	< 1	Very high
10–100	1–2	High
100–1000	2–3	Moderate
1000–10000	3–4	Low
˃ 10,000	˃ 4	Very low

Fig. 11. Table 8 showed that approximately 50% of the sounding stations showed moderate susceptibility to contamination. The results obtained are in consonance with those generated from the Dar-Zarrouk parameter and GOD model indices, and showed that in general, the aquifer has moderate susceptibility to contamination. These results

Table 8 Measures of AVI obtained at the vertical electrical sounding stations

VES Stations	Co-ordinates		Hydraulic conductivity K (m/day)		Hydraulic resistance C	AVI	Vulnerability rating
	Latitude (◦)	Longitude (◦)	Layer 1	Layer 2			
1	4° 37′ 9.4″	7° 4.6′ 43.56″	1.69590731	4.744688083	1184.519	3.073542	Low
2	4° 37′ 6.0″	7° 4.6′ 43.6″	2.80948183	1.132266473	1122.501	3.050187	Low
3	4° 37′ 15.5″	7° 4.6′ 39.97″	2.72423522	5.189549564	442.7822	2.64619	Moderate
4	4° 37′ 13.7″	7° 4.6′ 42.3″	1.91177491	2.693387767	4427.59	3.646167	Low
5	4° 37′ 24.2″	7° 4.6′ 32.1″	2.69338777	0.837464857	12,673.04	4.102881	Very low
6	4° 37′ 16.6″	7° 4.6′ 18.9″	2.04312475	11.05892217	602.6849	2.78009	Moderate
7	4° 37′ 17.4″	7° 46′ 11.4″	1.22674979	2.442603595	4376.595	3.641136	Low
8	4° 37′ 12.3″	7° 46′ 29.9″	3.5040743	0.795693866	8365.315	3.922482	Low
9	4° 37′ 5.9″	7° 46′ 35.5″	3.10481122	6.98535014	905.2528	2.95677	Moderate
10	4° 37′ 15.3″	7° 46′ 39.7″	21.8685738	11.21043915	130.3757	2.115197	Moderate
11	4° 37′ 15.8″	7° 46′ 41.4″	7.88098655	1.517548774	3729.103	3.571604	Low
12	4° 37′ 15.5″	7° 46′ 40.9″	15.1640051	5.277915092	950.7983	2.978088	Moderate
13	4° 37′ 15.3″	7° 46′ 39.7″	21.8685738	13.43472389	111.901	2.048834	Moderate
14	4° 37′ 14.7″	7° 46′ 37.29″	9.52082741	2.148500801	7311.634	3.864014	Low
15	4° 37′ 13.8″	7° 46′ 35.9″	7.50339692	1.64878757	4086.405	3.611341	Low
16	4° 37′ 13.3″	7° 46′ 35.2″	4.43116582	2.486260259	2623.989	3.418962	Low
17	4° 37′ 17.5″	7° 46′ 27.7″	21.0308718	8.984421456	158.2461	2.199333	Moderate
18	4° 37′ 16.5″	7° 46′ 22.5″	2.75043837	20.37081286	372.8045	2.571481	Moderate
19	4° 37′ 16.5″	7° 46′ 19.2″	16.2479015	75.86678919	54.38424	1.735473	High
20	4° 37′ 15.3″	7° 46′ 44.1″	14.9571325	12.29868058	531.6994	2.725666	Moderate

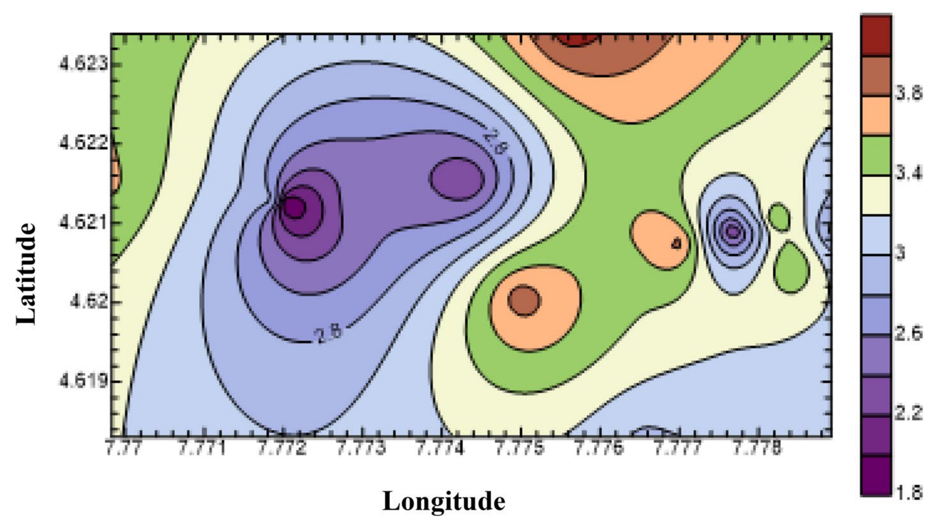

Fig. 11 Spatial distribution map of AVI model values

have illustrated the efficacy of geo-electrical technology in the delineation of aquifer protectivity, vulnerability, and soil corrosivity.

5 Conclusion

Surficial geophysical surveys were undertaken within a coastal milieu to investigate aquifer vulnerability to contamination. Primary geo-electrical indices were obtained from VES data, and 2D ERT surveys were undertaken to complement information derived from the soundings. To appraise aquifer vulnerability, longitudinal conductance measures were obtained, and the values ranged from 0.0071–1.95 mhos, with a mean of 0.32 mhos, indicating moderate aquifer protectivity. Soil corrosivity was evaluated using topsoil resistivity measures and results indicated moderate corrosivity within the area. Indexed-based modeling methods GOD and AVI were used to complement information obtained about aquifer protectivity. Measures of GOD and AVI, alongside their iso-parametric maps, indicated how aquifer vulnerability varied spatially across the study area. The GOD and AVI indices indicated that the region had moderate aquifer susceptibility to contamination. This was a possible result of arenite-argillaceous intercalations, which served as a protective seal over the aquifer. These results corroborated those obtained from longitudinal conductance indices which had indicated that the aquifer system had average protectivity. Anthropogenic pollutants in the region include industrial and domestic wastes, and agricultural pollutants such as pesticides, herbicides, insecticides, hence this work will aid in development of strategies for pollutant mitigation. Further, it will aid policy makers in developing effective aquifer monitoring and conservation stratagems.

Author contributions N.U.: study conception and design, data collection N.U., A.E., and N.J: data analysis and interpretation of results All authors reviewed the results and approved the final version of the manuscript.

Data availability All relevant data are included in the paper or its Supplementary Information.

Declarations

Competing interests The authors have no competing interests to declare that are relevant to the content of this article.

References

1. Yang D, Yang Y, Xia J. Hydrological cycle and water resources in a changing world: a review. Geography and Sustainability. 2021;2(2):115–22. https://doi.org/10.1016/j.geosus.2021.05.003.
2. Keller EA. Environmental geology. 9th ed. Pearson Prentice Hall. Upper Saddle River; 2011.
3. Amiaz Y, Sorek S, Enzel Y, Dahan O. Solute transport in the vadose zone and groundwater during flash floods. Water Resour Res. 2011. https://doi.org/10.1029/2011wr010747.
4. Montgomery CW, Szablewski GS. Environmental geology. 12th ed. New York: McGraw Hill LLC; 2024.
5. Plummer CC, Carlson DH, Hammersley L. Physical geology. 17th ed. New York: McGraw Hill LLC; 2022.
6. Inim IJ, Udosen NI, Tijani MN, Affiah UE, George NJ. Time-lapse electrical resistivity investigation of seawater intrusion in coastal aquifer of Ibeno, Southeastern Nigeria. Appl Water Sci. 2020;10(11):1–12. https://doi.org/10.1007/s13201-020-01316-x.
7. Udosen NI. Geo-electrical modeling of leachate contamination at a major waste disposal site in south-eastern Nigeria. Model Earth Syst Environ. 2022;8(1):847–56. https://doi.org/10.1007/s40808-021-01120-9.
8. Nalbantcilar MT. Assessment of the vulnerability potential for an unconfined aquifer in Konya Province, Turkey. In: Integrated waste management, vol. 2. IntechOpen; 2011. https://doi.org/10.5772/22339.
9. Braga ACDO, Francisco RF. Natural vulnerability assessment to contamination of unconfined aquifers by longitudinal conductance–(s) method. J Geogr Geol. 2014;6(4):68–79. https://doi.org/10.5539/jgg.v6n4p68.
10. Udosen NI, Ekanem AM, Thomas JE. Evaluation and modeling of a major coastal aquifer's vulnerability to contamination with the use of GOD and AVI models as indicators in South-eastern Nigeria. Res J Sci Technol. 2023;3(4):61–78.
11. George NJ, Ekanem AM, Thomas JE, Udosen NI, Ossai NM, Atat JG. Electro-sequence valorization of specific enablers of aquifer vulnerability and contamination: a case of index-based model approach for ascertaining the threats to quality groundwater in sedimentary beds. HydroResearch. 2024;7:71–85. https://doi.org/10.1016/j.hydres.2023.11.006.
12. Ekanem AM, Udosen NI. Hydrogeochemical–geophysical investigations of groundwater quality and susceptibility potential in Ikot Ekpene-Obot Akara Local Government Areas, Southern Nigeria. Water Pract Technol. 2023;18(11):2675–704. https://doi.org/10.2166/wpt.2023.187.
13. Foster SSD. Fundamental concepts in aquifer vulnerability, pollution risk and protection strategy. In: Duijvenbooden WV, Waegeningh HV. Vulnerability of soil and groundwater to pollutants: international conference Noordwijk ann Zee, The Netherlands, March 30–April 3; 1987. The Hague: TNO Committee on Hydrological Research; 1987.
14. Ekanem AM. AVI-and GOD-based vulnerability assessment of aquifer units: a case study of parts of Akwa Ibom State, Southern Niger Delta, Nigeria. Sustain Water Resour Manag. 2022;8(1):29. https://doi.org/10.1007/s40899-022-00628-x.
15. Obiora DN, Ajala AE, Ibuot JC. Evaluation of aquifer protective capacity of overburden unit and soil corrosivity in Makurdi, Benue state, Nigeria, using electrical resistivity method. J Earth Syst Sci. 2015;124:125–35. https://doi.org/10.1007/s12040-014-0522-0.

16. Foley D, McKenzie GD, Utgard RO. Investigations in environmental geology. 3rd ed. Upper Saddle River: Pearson Prentice Hall; 2009.
17. Udosen NI, Ekanem AM, Thomas JE. Geo-hydraulic characterization of a coastal aquifer system in South-eastern Nigeria with the inverse slope method. Res J Scie Technol. 2024;4(1):1–20.
18. Zohdy AA, Martin P, Bisdorf RJ. A study of seawater intrusion using direct-current soundings in the southeastern part of the Oxnard Plain, California (vol. 93, No. 524). US Geological Survey; 1993. https://doi.org/10.3133/ofr93524
19. Mbinkong RS, Kengni SHP, Ndoh NE, Gaetan TDN, Pokam BPG, Tabod CT. Evaluation of groundwater potential, aquifer parameters and vulnerability using geoelectrical method: a case study of parts of the Sanaga Maritime Division, Douala, Cameroon. Model Earth Syst Environ. 2024. https://doi.org/10.1007/s40808-023-01932-x.
20. George NJ, Ekanem AM, Ibanga JI, Udosen NI. Hydrodynamic implications of aquifer quality index (AQI) and flow zone indicator (FZI) in groundwater abstraction: a case study of coastal hydro-lithofacies in South-eastern Nigeria. J Coast Conserv. 2017;21:759–76. https://doi.org/10.1007/s11852-017-0535-3.
21. Udosen NI, Potthast R. Automated optimization of electrode locations for electrical resistivity tomography. Model Earth Syst Environ. 2018;4:1059–83. https://doi.org/10.1007/s40808-018-0472-7.
22. George NJ, Ekanem KR, Ekanem AM, Udosen NI, Thomas JE. Generic comparison of ISM and LSIT interpretation of geo-resistivity technology data, using constraints of ground truths: a tool for efficient explorability of groundwater and related resources. Acta Geophys. 2022;70(3):1223–39. https://doi.org/10.1007/s11600-022-00794-8.
23. George NJ. Integrating hydrogeological and second-order geo-electric indices in groundwater vulnerability mapping: a case study of alluvial environments. Appl Water Sci. 2021;11(7):123. https://doi.org/10.1007/s13201-021-01437-x.
24. Adeniji AE, Omonona OV, Obiora DN, Chukudebelu JU. Evaluation of soil corrosivity and aquifer protective capacity using geoelectrical investigation in Bwari basement complex area, Abuja. J Earth Syst Sci. 2014;123:491–502. https://doi.org/10.1007/s12040-014-0416-1.
25. Röttger B, Kirsch R, Scheer W, Thomsen S, Friborg R, Voss W. Multi-frequency airborne EM surveys—a tool for aquifer vulnerability mapping. In: Butler DK, editor. Near surface geophysics, investigations in geophysics No 13, society of engineering geophysicists; 2005. p. 643–651. https://doi.org/10.1190/1.9781560801719.ch26
26. Netto LG, Guimarães CC, Barbosa AM, Gandolfo OCB. Investigation of the contamination behavior in water and soil of an inactive dump from chemical analysis and geophysical method. Discov Geosci. 2024;2(1):1–14. https://doi.org/10.1007/s44288-024-00010-8.
27. Udosen NI, Ekanem AM, George NJ. Modeling of aquifer geo-hydraulic characteristics with geo-electrical methods at a major coastal aquifer system in Uyo, southern Nigeria. Water Pract Technol. 2024. https://doi.org/10.2166/wpt.2024.018.
28. Ekanem AM, Udosen NI. Evaluation of groundwater potentiality and quality in Ikot Ekpene-Obot Akara Local Government Areas, Southern Nigeria. Environ Contam Rev. 2023;6(1):46–57. https://doi.org/10.26480/ecr.01.2023.46.57.
29. Udosen NI, George NJ. Characterization of electrical anisotropy in North Yorkshire, England using square arrays and electrical resistivity tomography. Geomech Geophys Geo-Energy Geo-Resour. 2018;4:215–33. https://doi.org/10.1007/s40948-018-0087-5.
30. Udosen NI, Ekanem AM, George NJ. Geophysical exploration to assess leachate percolation and aquifer protectivity within hydrogeological units at a major open dump in Eket, Nigeria. Results Earth Sci. 2024;2: 100022. https://doi.org/10.1016/j.rines.2024.100022.
31. Benson AK, Payne KL, Stubben MA. Mapping groundwater contamination using dc resistivity and VLF geophysical methods; a case study. Geophysics. 1997;62(1):80–6. https://doi.org/10.1190/1.1444148.
32. Aristodemou E, Thomas-Betts A. DC resistivity and induced polarisation investigations at a waste disposal site and its environments. J Appl Geophys. 2000;44(2–3):275–302. https://doi.org/10.1016/s0926-9851(99)00022-1.
33. Braga ACDO, Malagutti Filho W, Dourado JC. Resistivity (DC) method applied to aquifer protection studies. Revista Brasileira de Geofísica. 2006;24:573–81. https://doi.org/10.1590/s0102-261x2006000400010.
34. Okoroh DO, Ibuot JC. Assessment of aquifer properties, protectivity and corrosivity using resistivity method: a case study of Federal College of Education (Technical), Omoku. Int J Energy Water Resour. 2023. https://doi.org/10.1007/s42108-023-00247-y.
35. Keller GV, Frischknecht FC. Electrical methods in geophysical prospecting. New York: Pergamon Press; 1966.
36. Ghazavi R, Ebrahimi Z. Assessing groundwater vulnerability to contamination in an arid environment using DRASTIC and GOD models. Int J Environ Sci Technol. 2015;12:2909–18. https://doi.org/10.1007/s13762-015-0813-2.
37. Udosen NI, George NJ. A finite integration forward solver and a domain search reconstruction solver for electrical resistivity tomography (ERT). Model Earth Syst Environ. 2018;4:1–12. https://doi.org/10.1007/s40808-018-0412-6.
38. Atakpo EA, Ayolabi EA. Evaluation of aquifer vulnerability and the protective capacity in some oil producing communities of western Niger Delta. Environmentalist. 2009;29:310–7. https://doi.org/10.1007/s10669-008-9191-3.
39. Naudet V, Revil A, Rizzo E, Bottero JY, Bégassat P. Groundwater redox conditions and conductivity in a contaminant plume from geoelectrical investigations. Hydrol Earth Syst Sci. 2004;8(1):8–22. https://doi.org/10.5194/hess-8-8-2004.
40. George NJ, Ibuot JC, Ekanem AM, George AM. Estimating the indices of inter-transmissibility magnitude of active surficial hydrogeologic units in Itu, Akwa Ibom State, Southern Nigeria. Arab J Geosci. 2018;11:1–16. https://doi.org/10.1007/s12517-018-3475-9.
41. Javed U, Kumar P, Hussain S, Nawaz T, Fahad S, Ashraf S, Ali K. Geospatial analysis of soil resistivity and hydro-parameters for groundwater assessment. Discov Geosci. 2024;2(1):3. https://doi.org/10.1007/s44288-024-00004-6.
42. Oroji B. Groundwater vulnerability assessment with using GIS in Hamadan-Bahar plain, Iran. Appl Water Sci. 2019;9(8):1–13. https://doi.org/10.1007/s13201-019-1082-x.
43. Helsel DR, Hirsch RM. Statistical methods in water resources, vol. 49. Elsevier; 1992. https://doi.org/10.1016/s0166-1116(08)x7035-9.
44. Kazakis N, Voudouris K. Comparison of three applied methods of groundwater vulnerability mapping: a case study from the Florina basin, Northern Greece. In: Advances in the research of aquatic environment, vol. 2. Berlin: Springer; 2011. p. 359–67. https://doi.org/10.1007/978-3-642-24076-8_42.
45. Falowo O, Ojo O. Groundwater assessment and aquifer vulnerability studies of Emure Ile, Southwestern Nigeria. Br J Appl Sci Technol. 2016;18(2):1–16. https://doi.org/10.9734/bjast/2016/29608.
46. Mfonka Z, Ngoupayou JN, Ndjigui PD, Kpoumie A, Zammouri M, Ngouh AN, Mouncherou OF, Rakotondrabe F, Rasolomanana EH. A GIS-based DRASTIC and GOD models for assessing alterites aquifer of three experimental watersheds in Foumban (Western-Cameroon). Groundw Sustain Dev. 2018;7:250–64. https://doi.org/10.1016/j.gsd.2018.06.006.

47. Henriet JP. Direct applications of the Dar Zarrouk parameters in ground water surveys. Geophys Prospect. 1976;24(2):344–53. https://doi.org/10.1111/j.1365-2478.1976.tb00931.x.
48. Ekanem AM. Georesistivity modelling and appraisal of soil water retention capacity in Akwa Ibom State University main campus and its environs, Southern Nigeria. Model Earth Syst Environ. 2020;6(4):2597–608. https://doi.org/10.1007/s40808-020-00850-6.
49. George NJ, Ibanga JI, Ubom AI. Geoelectrohydrogeological indices of evidence of ingress of saline water into freshwater in parts of coastal aquifers of Ikot Abasi, southern Nigeria. J Afr Earth Sc. 2015;109:37–46. https://doi.org/10.1016/j.jafrearsci.2015.05.001.
50. Mbipom EW, Okwueze EE, Onwuegbuche AA. Estimation of transmissivity using VES data from the Mbaise area of Nigeria. Niger J Phys. 1996;85:28–32.
51. Avbovbo AA. Tertiary lithostratigraphy of Niger delta. AAPG Bull. 1978;62(2):295–300. https://doi.org/10.1306/c1ea482e-16c9-11d7-8645000102c1865d.
52. Reijers TJA, Petters SW. Depositional environments and diagenesis of Albian carbonates on the Calabar Flank, SE Nigeria. J Pet Geol. 1987;10(3):283–94. https://doi.org/10.1111/j.1747-5457.1987.tb00947.x.
53. Short KC, Stauble AJ. Outline of geology of Niger Delta. AAPG Bull. 1967;51(5):761–79. https://doi.org/10.1306/5d25c0cf-16c1-11d7-8645000102c1865d.
54. Stacher P. Present understanding of the Niger Delta hydrocarbon habitat. In: Geology of deltas; 1995. p. 257–67.
55. Udosen NI, Potthast RWE, Astin TR. A domain search reconstruction algorithm for electrical resistivity tomography. In: 75th EAGE conference & exhibition incorporating SPE EUROPEC 2013. European association of geoscientists & engineers, June 2013, London, United Kingdom; 2013. p. cp-348. https://doi.org/10.3997/2214-4609.20130960
56. Udosen N, Potthast R. A framework for solving meta inverse problems: experimental design and application to an acoustic source problem. Model Earth Syst Environ. 2019;5:519–32. https://doi.org/10.1007/s40808-018-0541-y.
57. Udosen NI, Potthast RWE, Astin TR. Novel framework for finding optimal measurement locations. In: 73rd EAGE conference and exhibition incorporating SPE EUROPEC 2011. European Association of geoscientists & engineers, May 2011, Vienna, Austria; 2011. p. cp-238. https://doi.org/10.3997/2214-4609.20149569
58. Udosen NI, Potthast RWE, Astin TR. Automated optimisation of electrode locations to image 2D resistivity anomalies. In: 75th EAGE conference & exhibition incorporating SPE EUROPEC 2013. European association of geoscientists & engineers, June 2013, London, United Kingdom; 2013. p. cp-348. https://doi.org/10.3997/2214-4609.20130966
59. Udosen NI, Ekanem AM, George NJ. Appraisal of flood-prone litho-stratigraphic units via geo-electrical technology. Malay J Geosci. 2024;8(1):33–44. https://doi.org/10.26480/mjg.01.2024.33.44.
60. Oladapo MI, Mohammed MZ, Adeoye OO, Adetola BA. Geoelectrical investigation of the Ondo state housing corporation estate Ijapo Akure, Southwestern Nigeria. J Min Geol. 2004;40(1):41–8. https://doi.org/10.4314/jmg.v40i1.18807.
61. Akintorinwa OJ, Abiola O. Subsoil evaluation for pre-foundation study using geophysical and geotechnical approach. J Emerg Trends Eng Appl Sci. 2011;2(5):858–63.
62. Agunloye O. Soil aggressivity along steel pipeline route at Ajaokuta southwestern Nigeria. J Mining Geol. 1984;21:97–101.
63. Baeckmann WV, Schwenk W. Handbook of cathodic protection: the theory and practice of electrochemical corrosion protection technique. UK: Cambridge Press; 1975.
64. Stempvoort DV, Ewert L, Wassenaar L. Aquifer vulnerability index: a GIS-compatible method for groundwater vulnerability mapping. Can Water Resour J. 1993;18(1):25–37. https://doi.org/10.4296/cwrj1801025.